

## CHAPTER 1

### INTRODUCTION TO FAST BEAM-FOIL SPECTROSCOPY

The energy levels and spectra of free atoms and ions have been studied for many years. The physical quantities of interest include transition wavelengths, excitation and ionization energies, as well as fine- and hyperfine structure separations. More recently it has also become possible to make accurate determinations of the lifetimes of excited states in atoms and ions and their related quantities, atomic transition probabilities. All this experimental information is of great interest in atomic theory, for instance for understanding the electron correlation and relativistic effects on atomic structure. There are also important applications of the atomic data in astrophysics, as well as in plasma physics, research towards controlled thermonuclear fusion, and even in X-ray absorption fine structure (XAFS) of nano-particles and quantum computers.

A variety of experimental techniques have been developed for research in modern atomic physics. One of the most versatile and powerful methods uses fast beams of ions from accelerators. This method, usually called beam-foil spectroscopy (BFS) or fast beam-foil spectroscopy (FBS), was discovered in 1960 by Kay [1] and Bashkin [2]. These two authors independently realized the significance of directing ions from, e.g., van de Graaff accelerators, through a

thin carbon foil and making spectral studies of the light emitted from the subsequent decay processes. The initial work thus showed that the light predominantly originated from the accelerated ions and not from ejected foil particles or rest-gas excitation. By accelerating various elements different line spectra were obtained. The foil-excited ion beam forms a light source for atomic spectroscopy. Unlike most other such sources beam-foil spectroscopy also possesses excellent time resolution that allows studies of atomic lifetimes. This possibility was already realized in the early work [1,2].

The method of fast beam-foil spectroscopy has subsequently developed into a standard technique in contemporary atomic physics and has yielded valuable experimental data on transition wavelengths, excitation and ionization energies, fine- and hyperfine structure, Lande g factors, atomic lifetimes and transition probabilities, autoionization rates, and Lamb shifts.

Perhaps the most important property of the foil-excited beam is its spatial and thus temporal resolution. The place of excitation is extremely well defined at the foil and, since the velocity of the ions is usually known with an uncertainty of about 1 % or less, the time scale of excited ions is accurately known. On the other hand, the excitation process in beam-foil spectroscopy is quite abrupt (typically  $10^{-14}$  s or less) and as a result the atoms or ions are not prepared in eigenstates (solutions to time-independent Schrödinger equation) but in linear, coherent superpositions of eigenstates. The ion-foil interaction frequently results in non-statistical population of magnetic sublevels. Effects such as orientation (vector polarization) or alignment (tensor polarization) can be observed by studying the polarization of the emitted light.

While most of the work that has been performed has used relatively straightforward beam-foil spectroscopy techniques, several important modifications have also been made in recent years. The fast ions can be excited in a gas cell [3-5], and this method is also applicable to studies of atomic spectra and lifetimes. Furthermore, the ions from accelerator can be excited by a laser (e.g., a tunable dye laser) [6], which leads to selective population of the excited states. The beam-foil spectroscopy has been proven to be still a powerful method to investigate the micro structure of free atoms and ions.

The most obvious properties of the beam-foil spectroscopy light source have been briefly mentioned above. Additional and more detailed information can be found in chapter 4 and in many references [7-12].

The main aim of this work is to give a perspective of the current understanding and to present our new results for the doubly excited sextet states  $1s2s2p^23l \ ^6L$  and  $1s2p^33l \ ^6L'$ ,  $l=s, p, d$  in five-electron systems, and most particularly in O IV.

Experimentally, these levels are difficult to observe by conventional spectroscopy techniques, such as the high voltage discharge in gas cell method, because they lie well above several ionization limits of the five-electron singly excited states. Even though they are metastable against autoionization (see chapter 2), they usually de-excite and disappear by collisions with other ions without radiative transitions. Only the fast beam-foil technique allows straightforward observation of the radiative transitions produced by these sextet states [13,14]. The sextet states  $1s2s2p^23l \ ^6L$  and  $1s2p^33l \ ^6L$ ,  $l=s, p, d$ , in the boron isoelectronic sequence are well above several ionization levels and metastable against electric-dipole radiation decay to singly excited five-electron states and

against Coulomb autoionization into the adjacent continua  $1s^2 2l_1 2l_2 n l \ ^4L$  due to different spin multiplicity (see chapter 2). Thus the main decay channel is electric-dipole radiation in the fast beam-foil experiments. In 1992, beam-foil spectroscopy [15,16] was used to provide initial data on low-lying sextet states in doubly excited boron-like nitrogen, oxygen and fluorine.

Using fast beam-foil spectroscopy, the recent work of Lapierre and Knystautas [17] on possible sextet transitions in Ne VI highlights the significance in this sequence. They measured several excitation energies and lifetimes. Some of the fine structures of individual  $1s2s2p^2 3s \ ^6P_J$  were resolved and measured in O IV, FV and Ne VI by this work [18]. There are no further results reported for transitions from highly excited sextet states in any five-electron atoms or ions.

In this work, the fast beam-foil spectra of oxygen were recorded at a Van de Graaff accelerator at University of Liège using a Seya-nomioka grating incidence spectrometers. The  $1s2s2p^2 3l \ ^6L - 1s2p^3 3l \ ^6L'$ ,  $l=s, p, d$ , electric-dipole transitions between sextet states in O IV have been searched for in these spectra and in spectra previously recorded at University of Lyon and Argonne National Laboratory. At the same time we also found and reassigned some new electric-dipole transitions in doubly excited O V.

## CHAPTER 2

### MULTIPLY EXCITED STATES IN OXYGEN, FLUORINE AND NEON

Most atomic energy levels where only a single electron is excited from the ground state are below the first ionization limit of the atomic ion being studied. In the early 1970s the technique of fast beam spectroscopy enabled efficient studies of atomic states with more than one electron excited. These multiply excited states (denoted by  $A^{**}(^{2S+1}L_J^P)$ ) typically have energies above the first ionization limit, and most such states autoionize by electrostatic (Coulomb) interaction very rapidly (in about  $10^{-14}$  seconds) by emitting an electron, and leaving the atom ionized (denoted by  $A^+(^{2S'+1}L'_J{}^{P'})$ ) (in the case of an ion, with a charge one unit higher).



The selection rules for this process are  $\Delta J=0$  (and  $\Delta S=\Delta L=0$  within the LS coupling) and no parity change ( $\Delta P=0$ ). However, in the doubly excited sextet states of boron-like atoms there are no final states that fulfill these requirements. Thus they are metastable against dipole-radiation decay to singly excited five-electron states and against autoionization decay to singly excited four-electron state continua [15,19]. They can decay by autoionization via spin-orbit, spin-other-orbit or spin-spin interactions. However, the probabilities of these

processes are several orders of magnitude lower than for the electrostatic (Coulomb) autoionization.

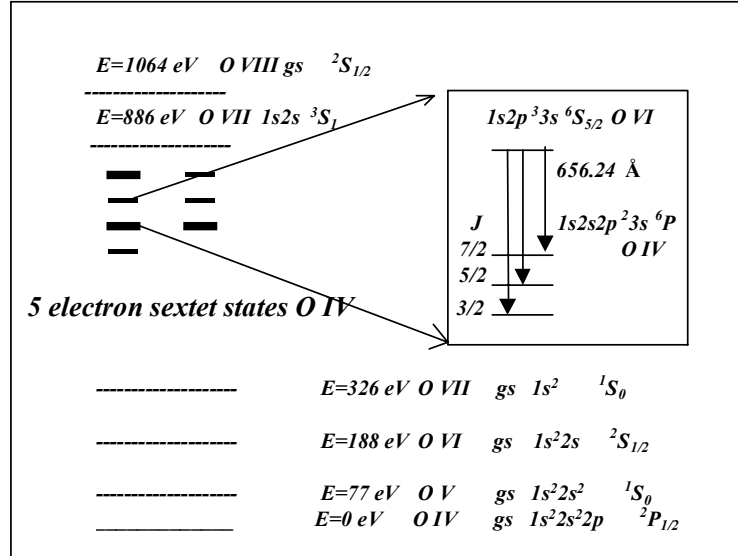


FIG. 2.1. Term diagram of the doubly excited sextet states of O IV. The mean wavelength for  $1s2s2p^23s\ ^6P-1s2p^33s\ ^6S^o$  transitions in O IV is shown. The energies are not to scale.

In Fig. 2.1 we show an overview of excitation energies of several ionization stages above the ground state of the five-electron oxygen ion. The level structures of other isoelectronic ions (such as F V and Ne VI) are similar, and their energies scale according to their nuclear charges. The sextet levels of O IV have these very high energies, principally due to the 1s and 2s electron vacancies (such atoms have been termed "hollow atoms"). These 5-electron high-spin states have energies typically just below the 2-electron O VII 1s2s and 1s2p states, more than 0.8 keV above the O IV ground state. The same configurations also yield quartet and doublet states that decay rapidly by x-ray

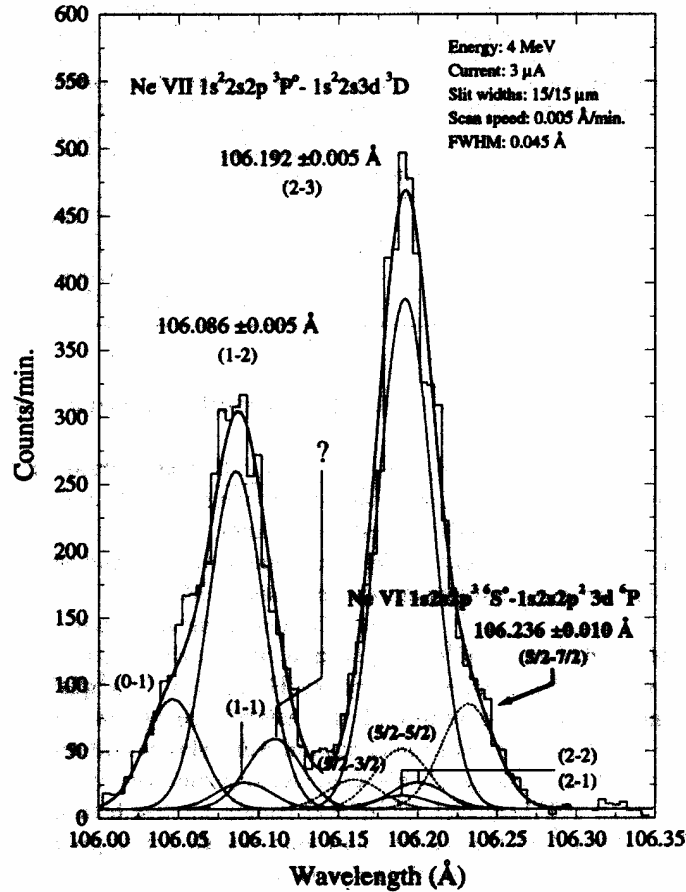
emission (energies of the order of 0.8 keV in oxygen). The x-ray emission will compete with auger-electron processes, but will tend to dominate more for the more highly charged ions of the isoelectronic sequence. In boron-like systems excited sextet states do not autoionize by Coulomb interaction, but make radiative transitions to lower states. Radiative decays (with  $10^8$ - $10^{10}$  s<sup>-1</sup> rates) then form an alternate decay possibility and allow investigation of the multiply excited states. The lifetimes for the lowest sextet states of boron-like O IV are about  $10^{-6}$  second, and the higher-lying states have typically  $10^{-10}$  second lifetimes. Since these doubly excited sextet states of boron-like O IV, F V and Ne VI are metastable and have energies well above several ionization levels, they are possible candidates for XUV- and soft x-ray lasers and for energy storage.

It has been found that fast beam-foil spectroscopy is very efficient in populating multiply excited states [15-18], and their decay can be observed by photon spectroscopy in emission.

The recent work of Lapierre and Knystautas [17] on possible sextet transitions in Ne VI highlights the significance but also difficulties in this sequence. They obtained the very best resolution ever achieved in a beam-foil spectrum in the grazing incidence region, but their tentative identifications of the two transitions at 12.0 and 10.6 nm show rather weak lines and overwhelming blending problems as shown in Fig. 2.2. The work of Blanke *et al.* [15] in searching for the same two sextet transitions in C III, O IV and F V indicates blending problems in almost all cases (see Fig. 2.3). Hence, all these identifications depend sensitively on the accuracy of the various calculations. Given this uncertainty in the identifications of all sextet transitions in the

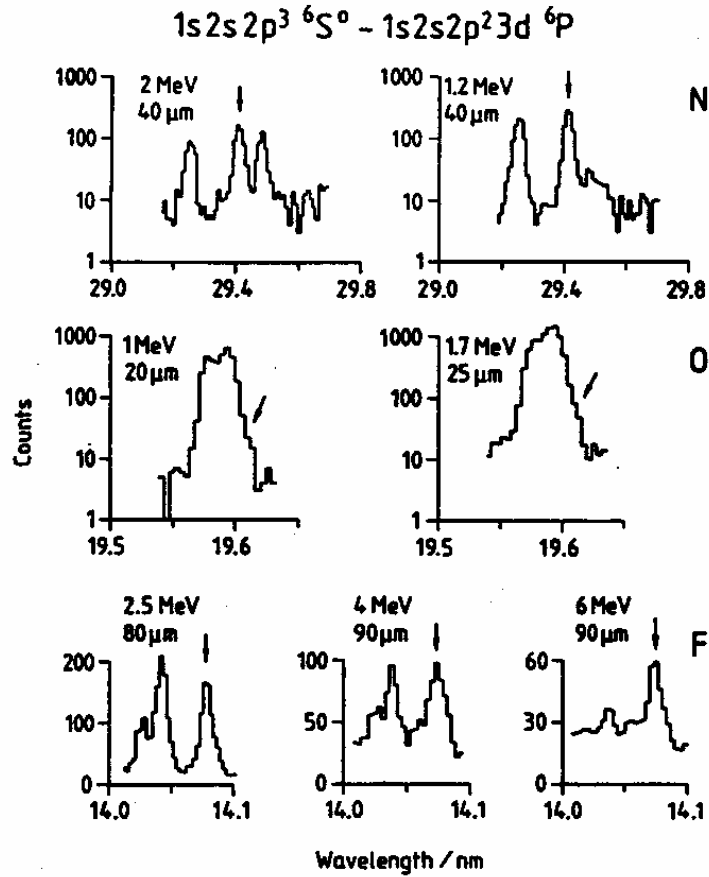
isoelectronic sequence, it is desirable to find unambiguous experimental verification of the calculations, and also to compare with improved theoretical calculations.

*A Lapierre and É J Knystautas*



The Gaussian deconvolution of the fine-structure transitions from Ne vi  $1s^2 2s 2p^3 P^\circ - 1s^2 2s 3d^3 D$  in this high-resolution spectrum cannot reproduce conveniently this region without introducing a spectral line in the high-wavelength slope of (2-3). This line might be the sextet fine-structure component Ne vi  $1s 2s 2p^3 {}^6S_{3/2} - 1s 2s 2p^2 3d {}^6P_{7/2}$  while  $(\frac{5}{2} - \frac{3}{2})$  and  $(\frac{3}{2} - \frac{3}{2})$  would be blended with (2-3).

FIG. 2.2. The recent work of Lapierre and Knystautas [17] on possible sextet transitions in Ne VI highlights the significance and difficulties in this sequence. The tentative identifications of the two transitions at 12.0 and 10.6 nm show rather weak lines and overwhelming blending problem. [The figure is taken from [17].]



The  $1s2s2p^3\ ^6S^0 - 1s2s2p^23d\ ^6P$  transition in beam-foil spectra of the elements N, O, and F, recorded at two to three different beam energies each. The spectrometer slit widths are given for each recording

FIG. 2.3. The work of Blanke et al. [15] in searching for the two possible sextet transitions in C III, O IV and F V indicates blending problems in all six cases. [The figure is taken from [15] .]

Most of the recent work on boron-like atoms has used CI methods, i.e. the Multi-Configuration Hartree-Fock method (MCHF) [15,17,18], Multi-Configuration Dirac-Fock method (MCDF) [15,18,21-24], or superposition-of-configurations Hartree-Fock relativistic method with the complex members (SOCHFR) [17]. For the sextet states in O IV, F V and Ne VI, the CI method is

still quite effective [15,16]. Hence, we can use a CI method to obtain accurate energies for the sextet states in O IV, F V and Ne VI. Our results will show the origins and size of the correlation energies. The CI values and energies of the sextet states depend sensitively on the configurations considered in the calculations. Generally more configurations are better for good precision [20].

In this work we have obtained the theoretical energy and wavelength data for the doubly excited sextet states in O IV, F V and Ne VI with both MCHF [20] and MCDF [21-24] methods. Experimentally, we have made new results using the fast-ion beam-foil technique for O IV, and using previous unpublished results for the F V and Ne VI spectra. The information from the experiments and theoretical studies greatly improves the understanding of the origin of the configuration interactions and correlation energies for the doubly-excited sextet states in O IV, F V and Ne VI.

We are able to clarify the origin of the differences between our theoretical transition energies and the experimental data: to obtain accurate energies for the doubly excited sextet states in O IV, F V and Ne VI, the QED effect and higher-order relativistic corrections cannot be neglected. These contributions from the QED and higher-order relativistic effects to the energy of the sextet states are calculated using the methods described by Chung [25-27].

## CHAPTER 3

### THEORY

In this work we have used two calculation methods: the first is the Multi-configuration Hartree-Fock (MCHF) method [20] with QED and higher-order relativistic corrections added, and the second is the Multi-configuration Dirac-Fock (MCDF) GRASP code [21-24]. In this chapter I present a brief overview of the MCHF (with QED and higher-order relativistic corrections) and MCDF approximations for the calculation of atomic states, energies and transition rates. Hartree atomic units,  $e=\hbar=m_e=1$  ( $\alpha=1/c$  for chapter 3.2), will be used throughout.

#### 3.1 The Multi-Configuration Hartree-Fock (MCHF) Method with the QED and Higher-order Relativistic Corrections

##### 3.1.1 Multi-Configuration Hartree-Fock Method

For a sextet state of a five-electron system  $n_1l_1^{w_1}n_2l_2^{w_2}n_3l_3^{w_3}n_4l_4^{w_4}n_5l_5^{w_5}{}^6L_J$ , where  $w_i = 0, 1, \dots$ , or  $2l_i + 1$ ,  $i=1, 2, \dots$  and 5, and  $\sum_{i=1}^5 w_i = 5$ , the wavefunction is

$$\Psi(\gamma, LS=5/2JM_J) = \sum_{i=1}^N c_i \Phi(\gamma_i, LS=5/2JM_J), \quad (3.1.1)$$

where  $c_i$  is configuration interaction coefficient,  $N$  is the total number of configurations with the same LSJM<sub>J</sub> and the same parity, label  $\gamma_i$  is all information such as configurations, orbital numbers, couplings, etc., to define the a configuration state function (CSF), the wavefunction for the sextet state with five-electron configuration  $\gamma_i$ , which is

$$\Phi(\gamma_i, \text{LSJM}_J) = \sum_{\beta} \langle \Phi(\beta, q) | \gamma_i, \text{LSJM}_J \rangle | \Phi(\beta, q) \rangle, \quad (3.1.2)$$

where  $\langle \Phi(\beta, q) | \gamma_i, \text{LSJM}_J \rangle$  is the Clebsch-Gordon coefficient,  $q$  is the spatial position of all five electrons, and

$$\Phi(\beta, q) = \frac{1}{\sqrt{N!}} A[\Phi(\beta_1, q_1) \Phi(\beta_2, q_2) \Phi(\beta_3, q_3) \Phi(\beta_4, q_4) \Phi(\beta_5, q_5)], \quad (3.1.3)$$

where  $A$  is the antisymmetrization operator. The one-electron wavefunction is

$$\Phi(\beta_i, q_j) = \frac{1}{r} P_{nl}(r_j) Y_{l, m_l}(\theta, \varphi) \chi_{m_s}(\sigma), \quad (3.1.4)$$

where  $\beta_i = (n \ l \ m_l \ m_s)$ , and  $P_{nl}(r_j)$  satisfies

$$\left( -\frac{d^2}{dr_i^2} + \frac{l(l+1)}{r_i^2} - \frac{2Z}{r_i} + \sum_{j < i} \frac{2}{r_{ij}} - \varepsilon_{nl} \right) P_{nl}(r_i) = 0. \quad (3.1.5)$$

The total Hamiltonian is the Breit-Pauli Hamiltonian

$$H_{BP} = H_{NR} + H_{RS} + H_{FS}, \quad (3.1.6)$$

where

$$H_{NR} = \sum_{i=1}^5 \left( -\frac{1}{2} \nabla_i^2 - \frac{Z}{r_i} \right) + \sum_{j < i} \frac{1}{r_{ij}} \quad (3.1.7)$$

is the zeroth-order non-relativistic Hamiltonian,

$$H_{RS} = H_{MC} + H_{D1} + H_{D2} + H_{OO} + H_{SSC} \quad (3.1.8)$$

is the relativistic shift Hamiltonian, where

$$H_{MC} = -\frac{\alpha^2}{8} \sum_{i=1}^5 (\nabla_i^2)^+ (\nabla_i^2) \quad (3.1.9)$$

is the mass correction term,

$$H_{D1} = -\frac{\alpha^2 Z}{8} \sum_{i=1}^5 \nabla_i^2 \left( \frac{1}{r_i} \right) \quad (3.1.10)$$

is the one-electron Darwin term,

$$H_{D2} = \frac{1}{4} \sum_{j<i}^5 \nabla_i^2 \left( \frac{1}{r_{ij}} \right) \quad (3.1.11)$$

is the two electron Darwin term,

$$H_{OO} = -\frac{\alpha^2}{2} \sum_{j<i}^5 \left[ \frac{\vec{P}_i \cdot \vec{P}_j}{r_{ij}} + \frac{\vec{r}_{ij} \cdot \vec{r}_{ij} \cdot \vec{P}_i \cdot \vec{P}_j}{r_{ij}^3} \right] \quad (3.1.12)$$

is the orbit-orbit term, and

$$H_{SSC} = -\frac{3\pi\alpha^2}{8} \sum_{j<i}^5 (\vec{S}_i \cdot \vec{S}_j) \delta(\vec{r}_i \cdot \vec{r}_j) \quad (3.1.13)$$

is the spin-spin contact term. The fine-structure operator is

$$H_{FS} = H_{SO} + H_{SOO} + H_{SS} \quad , \quad (3.1.14)$$

where

$$H_{SO} = -\frac{\alpha^2 Z}{2} \sum_{i=1}^5 \frac{1}{r_i^3} \vec{l}_i \cdot \vec{s}_i \quad (3.1.15)$$

is the spin-orbit term,

$$H_{SOO} = -\frac{\alpha^2}{2} \sum_{j<i}^5 \frac{\vec{r}_{ij} \times \vec{P}_i}{r_{ij}^3} \cdot (\vec{s}_i + 2\vec{s}_j) \quad (3.1.16)$$

is the spin-other-orbit term, and

$$H_{SS} = \alpha^2 \sum_{j<i}^5 \frac{1}{r_{ij}^3} [ \vec{s}_i \cdot \vec{s}_j - 3 \frac{(\vec{s}_i \cdot \vec{r}_{ij})(\vec{s}_i \cdot \vec{r}_{ij})}{r_{ij}^2} ] \quad (3.1.17)$$

is the spin-spin term. Then we solve the MCHF equation

$$H_{BP}\Psi=E\Psi, \quad (3.1.18)$$

where

$$H_{ij}=\langle \gamma_i,LSJM_J|H_{BP}|\gamma_j,LSJM_J\rangle, \quad (3.1.19)$$

and get the eigenvalue of energy  $E(\gamma, LS=5/2JM_J)$  for the sextet eigenstate  $\Psi(\gamma,LSJM_J)$ . The oscillator strength for the  $(\gamma_i L_iS_iJ_i) \rightarrow(\gamma_j L_jS_jJ_j)$  transition induced by a multipole radiation field operator  $O_M^{(k)}$  of order  $k$  is

$$f_{i \rightarrow j}^k = \frac{C_k(\alpha\omega)^{2k-1}}{\alpha g} \left| \langle \gamma_i L_i S_i J_i \| O^{(k)} \| \gamma_j L_j S_j J_j \rangle \right|^2, \quad (3.1.20)$$

where

$$g = 2J_i + 1, \quad (3.1.21)$$

$$C_k = \frac{(2k+1)(k+1)}{k((2k+1)!!)^2}. \quad (3.1.22)$$

The intensity of the spectral line, produced by the  $(\gamma_i L_iS_iJ_i) \rightarrow(\gamma_j L_jS_jJ_j)$  transition, is proportional to the weighted line strength  $gf$  value. The transition rate is

$$A_{ij}^k = 2\alpha\omega^2 f_{i \rightarrow j}^k. \quad (3.1.23)$$

The lifetime of the  $(\gamma_i L_iS_iJ_i)$  state is

$$\tau_i = \frac{1}{\sum_{k,j} A_{ij}^k}. \quad (3.1.24)$$

### 3.1.2 Higher-Order Relativistic Contributions and QED Effects

To obtain an accurate energy for the sextet state in five-electron oxygen, the quantum electrodynamics effect (QED) and higher-order relativistic contribution

cannot be ignored. We use the hydrogenic formula from [25-27] to estimate the quantum electrodynamics effect (QED) and higher-order relativistic contribution for the sextet state in five-electron oxygen. For an  $s$ -electron,

$$\begin{aligned} \Delta E_{QED}(n,0) = & \frac{4Z_{eff}^4 \alpha^3}{3\pi m^3} \left\{ \frac{19}{30} - 2 \ln(\alpha Z_{eff}) - \ln K(n,0) + 7.214 \alpha Z_{eff} - (\alpha Z_{eff})^2 [3 \ln^2(\alpha Z_{eff}) \right. \\ & \left. + 8.695 \ln(\alpha Z_{eff}) + 19.081] \right\}, \end{aligned} \quad (3.1.25)$$

For any other  $nl$  electron,

$$\begin{aligned} \Delta E_{QED}(n,l) = & \frac{4Z_{eff}^4 \alpha^3}{3\pi m^3} \left\{ \frac{3c_{l,j}}{8(2l+1)} - \ln K(nl) + (\alpha Z_{eff})^2 \ln(\alpha Z_{eff})^{-2} \left[ \left(1 - \frac{1}{n^2}\right) \left(\frac{1}{10} + \frac{1}{4} \delta_{j,1/2}\right) \delta_{j,l} \right. \right. \\ & \left. \left. + \frac{8(3 - l(l+1)/n^2)}{(2l-1)2l(2l+1)(2l+2)(2l+3)} \right] + \frac{3\alpha}{4\pi} (-0.3285)c_{l,j}/(2l+1) \right\}, \end{aligned} \quad (3.1.26)$$

$$\text{where } c_{l,j} = \begin{cases} l/(l+1) & \text{for } j = l+1/2 \\ -1/l & \text{for } j = l-1/2 \end{cases} \quad (3.1.27)$$

The values of  $\ln K(nl)$  are taken from Drake and Swainson [27]. The effective nuclear charge  $Z_{eff}$  is estimated as below. The energy eigenvalue of the one-electron Dirac equation for a coulomb potential is

$$E_{Dirac}(Z) = \frac{1}{\alpha^2} \left[ 1 + \left[ \frac{\alpha Z}{n - k + \sqrt{k^2 - \alpha^2 Z^2}} \right]^2 \right]^{-1/2} - \frac{1}{\alpha^2}, \quad (3.1.28)$$

where  $k=j+1$  for an hydrogenic electron. To order of  $\alpha^2 Z^4$ ,  $E_{Dirac}$  reduces to

$$E^{(1)}(Z) = -\frac{Z^2}{2n^2} \left[ 1 + \frac{\alpha^2 Z^2}{n} \left[ \frac{1}{k} - \frac{3}{4n} \right] \right], \quad (3.1.29)$$

Since we have calculated the energy of the  $n_5 l_5$  valence electron in the sextet state ( $n_1 l_1^{w1} n_2 l_2^{w2} n_3 l_3^{w3} n_4 l_4^{w4} n_5 l_5^{w5} {}^6L_J$ ) to the order of  $\alpha^2 Z^4$  with the eqs (3.1.1) to (3.1.19), we can define a  $Z_{eff}$  by

$$\begin{aligned}
& E(n_1 l_1^{w_1} n_2 l_2^{w_2} n_3 l_3^{w_3} n_4 l_4^{w_4} n_5 l_5^{w_5}, {}^6L_J) - E(n_1 l_1^{w_1} n_2 l_2^{w_2} n_3 l_3^{w_3} n_4 l_4^{w_4}, {}^5L'_{J'}) \\
& = -\frac{Z_{eff}^2}{2n_5^2} \left[ 1 + \frac{\alpha^2 Z_{eff}^2}{n_5} \left[ \frac{1}{k_5} - \frac{3}{4n_5} \right] \right], \tag{3.1.30}
\end{aligned}$$

where  ${}^5L'_{J'}$  is determined by the transition being studied, in which the energy of the valence electron changes. Using the  $Z_{eff}$ , an approximate  $\Delta E_{QED}(n_5, l_5)$  in the sextet state  $n_1 l_1^{w_1} n_2 l_2^{w_2} n_3 l_3^{w_3} n_4 l_4^{w_4} n_5 l_5^{w_5} {}^6L_J$  is estimated with eqs. (3.1.25) to (3.1.27). With the same  $Z_{eff}$  the higher-order relativistic contribution is estimated from

$$\Delta E_{HO}(n_5 l_5) = E_{Dirac}(Z_{eff}) - E^{(1)}(Z_{eff}). \tag{3.1.31}$$

In the same way we can obtain the QED and higher order relativistic effects,  $\Delta E_{QED}(n_i l_i j_i, \alpha LSJM_J)$  and  $\Delta E_{HO}(n_i l_i j_i, \alpha LSJM_J)$ ,  $i=1,2, \dots, 5$ , for all the electrons in the ion in the sextet states of the boron-like ions. The total energy of the sextet state is

$$E_T = E(\alpha, LSJM_J) + \sum_{i=1}^5 [\Delta E_{QED}(n_i l_i j_i, \alpha LSJM_J) + \Delta E_{HO}(n_i l_i j_i, \alpha LSJM_J)] \tag{3.1.32}$$

### 3.2 The Multi-Configuration Dirac-Fock (MCDF) Method

We also used the MCDF [21-24] program to calculate the energies, lifetimes and relevant E1 transitions of doubly excited sextet states of boron-like O IV, F V and Ne VI.

For a sextet state of a five-electron system  $n_1 l_1^{w_1} n_2 l_2^{w_2} n_3 l_3^{w_3} n_4 l_4^{w_4} n_5 l_5^{w_5} {}^6L_{JM_J}^P$ , where  $w_i = 0, 1, \dots$ , or  $2l_i + 1$ ,  $i=1,2, \dots$  and 5, and  $\sum_{i=1}^5 w_i = 5$ , the wavefunction is the atomic state function (ASF)

$$|\Gamma \text{ PJM}_J\rangle = \sum_{i=1}^N c_{i\Gamma} |\gamma_i \text{ PJM}_J\rangle, \quad (3.2.1)$$

where  $c_{i\Gamma}$  is configuration interaction coefficient,  $N$  is the total number of configurations with the same  $\text{JM}_J$  and the same parity  $P$ , the label  $\gamma_i$  has all information such as configurations, orbital numbers, couplings, etc., to define the configuration state function (CSF)

$$|\gamma_i \text{ PJM}_J\rangle = \sum_{n\kappa m} \langle n\kappa m, q | \gamma_i \text{ PJM}_J\rangle |n\kappa m, q\rangle, \quad (3.2.2)$$

uniquely, where  $\langle n\kappa m, q | \gamma_i \text{ PJM}_J\rangle$  is the Clebsch-Gordon coefficient related to the angular momentum couplings,  $q$  is the spatial position of all five electrons, and

$$|n\kappa m, q\rangle = \frac{1}{\sqrt{N!}} A \{ |n_1\kappa_1 m_1, q_1\rangle |n_2\kappa_2 m_2, q_2\rangle |n_3\kappa_3 m_3, q_3\rangle |n_4\kappa_4 m_4, q_4\rangle |n_5\kappa_5 m_5, q_5\rangle \}, \quad (3.2.3)$$

where  $A$  is the antisymmetrization operator.

$$|n_i\kappa_i m_i, q_i\rangle = \frac{1}{r} \begin{pmatrix} P_{n_i\kappa_i}(r_i) & \chi_{\kappa_i m_i}(\vec{r}_i / r_i) \\ iQ_{n_i\kappa_i}(r_i) & \chi_{-\kappa_i m_i}(\vec{r}_i / r_i) \end{pmatrix}, \quad (3.2.4)$$

is the one-electron Dirac orbital, where  $n_i$  is the principal quantum number,  $\kappa_i = \pm(j_i + 1/2)$  for  $l_i = j_i \pm 1/2$ ,  $m_i = -j_i, \dots, j_i$ , and  $P_{n_i\kappa_i}(r_i)$  and  $Q_{n_i\kappa_i}(r_i)$  are the large and small component radial wavefunctions, and

$$\chi_{\kappa_i m_i}(\vec{r}_i / r_i) = \sum_{\sigma = \pm 1/2} \langle l_i m_i - \sigma | l_i - 1/2, j_i m_i \rangle Y_{l_i, m_i - \sigma}(\theta_i, \varphi_i) \varphi^\sigma \quad (3.2.5)$$

are the spinor spherical harmonics, where  $\varphi^\sigma$  is a spinor basis function.

The total Hamiltonian is

$$H = H_{DC} + H_{TR} + H_{QED}, \quad (3.2.6)$$

where

$$H_{DC} = \sum_{i=1}^5 \left\{ \sum_{r=1}^3 \alpha_r \bar{p}_r + (\beta - 1)c^2 - \frac{Z}{r_i} \right\} + \sum_{j < i} \frac{1}{r_{ij}} \quad (3.2.7)$$

is the Dirac-Coulomb Hamiltonian, where  $\alpha_r, \beta$  are the Dirac matrix. The lowest-order correction to Coulomb interaction between two electrons, labelled  $i$  and  $j$ , due to the exchange of a single photon, is given by

$$H_{TR} = - \sum_{i < j} \left[ \sum_{\mu, \nu=1}^3 \alpha_{i\mu} \alpha_{j\nu} \left( \delta_{\mu, \nu} \frac{\cos(\omega R)}{R} - \frac{\partial^2}{\partial R_{i\mu} \partial R_{j\nu}} \frac{\cos(\omega R) - 1}{\omega^2 R} \right) \right], \quad (3.2.8)$$

where  $R = r_{ij}$ ,  $\omega = |\varepsilon_i - \varepsilon_j|/c$ . In the long-wavelength limit ( $\omega \rightarrow 0$ ) this reduces to the well-known Breit interaction. The QED effect is written as

$$H_{QED} = H_{SE} + H_{VP}, \quad (3.2.10)$$

where we only consider the diagonal matrix elements of the self-energy  $H_{SE}$  and the vacuum polarization correction  $H_{VP}$  in a hydrogenlike system:

$$H_{rr}^{SE} = \sum_{i=1}^5 (w_i)_r E_{n_i, \kappa_i}^{SE}, \quad (3.2.11)$$

$$E_{n_i, \kappa_i}^{SE} = \frac{Z_{eff_i}^4}{\pi c^3 n^3} \left\{ \begin{array}{ll} F_{n_i, \kappa_i}(Z_{eff_i}/c), & \text{for } 1s, 2s, 2p_{1/2}, \text{ and } 2p_{3/2} \text{ orbitals,} \\ F_{2\kappa_i}(Z_{eff_i}/c), & \text{for } ns, np_{1/2}, \text{ and } np_{3/2} \text{ orbitals, } n \geq 3, \\ 0, & \text{otherwise,} \end{array} \right\}, \quad (3.2.12)$$

and

$$H_{rr}^{VP} = \sum_{i=1}^5 (w_i)_r \int_0^{+\infty} dr V^{VP}(r) (P_{n_i, \kappa_i}^2(r) + Q_{n_i, \kappa_i}^2(r)), \quad (3.2.13)$$

where  $F_{n\kappa}(Z/c)$  are taken from [28-32] and  $V^{VP}(r)$  is the lowest order of the vacuum polarization correction, the short-range modification of nuclear field due to screening of virtual electron-positron pairs. We then solve the MCHF equation

$$H\Psi=E\Psi, \quad (3.2.15)$$

where

$$\Psi=|\Gamma \text{ PJM}_J\rangle, \quad (3.2.16)$$

$$H_{rs}=\langle \gamma_r \text{ PJM}_J | H | \gamma_s \text{ PJM}_J \rangle, \quad (3.2.17)$$

and obtain the eigenvalue of energy  $E(\Gamma \text{ PJM}_J)$  for the sextet eigenstate  $\Psi=|\Gamma \text{ PJM}_J\rangle$ . The oscillator strength for the transition from  $|\Gamma_i \text{ P}_i J_i\rangle$  to  $|\Gamma_j \text{ P}_j J_j\rangle$  induced by a multipole radiation field operator  $O_M^{(k)}$  of order  $k$  is

$$f_{i \rightarrow j} = \frac{\pi c}{(2J+1)\omega^2} \left| \langle \Gamma_i P_i J_i || O^{(L)} || \Gamma_j P_j J_j \rangle \right|^2. \quad (3.2.18)$$

We use (3.1.23) and (3.1.24) to calculate the electric dipole transition rates  $A_{ij}^k$  and the lifetimes  $\tau_i$ , and the  $gf_{i \rightarrow j}$  values.

### 3.3 Multi-Configuration Hartree-Fock (MCHF) Calculations and Results on Quintet States in Beryllium-like CIII, N IV, O V, FVI and Ne VII

In order to obtain information on the validity of our theoretical approach, we first calculated wavelengths and lifetimes of transitions that belong to doubly excited quintet states of four-electron CIII, N IV, O V, FVI and Ne VII ions. For comparison there exists a large amount of reliable experimental data, confirmed by elaborate calculations. We focused on the 2s-2p transitions and evaluated the differences between experimental and theoretical transition energies and lifetimes of the 2p states for all  $Z$  on which the data are available.

For the first step, we performed MCHF calculations with a single configuration, called SCHF here. In the SCHF calculations only those configurations corresponding to the levels desired were considered. Correlation

effects left out in the first SCHF calculations can be handled by adding further configurations belonging to the same (LSJM<sub>J</sub>P) just as the configuration being studied.

After updating the MCHF codes we performed the relativistic calculations with an initial expansion of up to 4000 CSFs and a full Pauli-Breit Hamiltonian matrix  $H$ . For a five-electron system the CI expansion generated by the active set leads to a large number of expansions. In order to reduce the number of the configurations, we chose the configurations  $n_1l_1n_2l_2n_3l_3n_4l_4n_5l_5$ , where  $n_i=1, 2, 3, 4$  and  $5$ ,  $l_i=0, \dots, \min(4, n_i-1)$ . We also included  $6s$  and  $6p$  electrons. We did not include the  $g$  electrons for the  $n=5$  shell. For the MCHF calculations of the ground  $1s2s2p^2\ ^5P_{J=1,2,3}$  quintet states in C III, N IV, O V, F VI, and Ne VII we chose  $1s, 2s, 2p, 3s, 3p$  and  $3d$  electrons to compose the configurations. For the  $1s2p^3\ ^5S$  state in C III, N IV, O V, F VI, and Ne VII we chose  $1s$  through  $4d, 4p, 4s, 3d, 3p$  electrons, respectively. After determining the radial wave functions we included the relativistic operators of mass correction, one- and two-body Darwin terms and the spin-spin contact term. The fine structure splitting is strongly involved in the experiments and identifications, and has been accurately measured. So we included the  $J$ -dependent fine structure operators, orbit-orbit term, spin-orbit term and spin-other-orbit term in both SCHF and MCHF calculations, which were not previously included in the calculations by Miecznik *et al.* [16].

We also used the MCDF [21-25] program to calculate the energies, lifetimes and relevant E1 transitions of doubly excited sextet of boron-like O IV, F V and Ne VI. To obtain better evaluations of the correlation energies of the two doubly-excited quintet states  $1s2s2p^2\ ^5P_{J=1,2,3}$  and  $1s2p^3\ ^5S$  in C III, N IV, O V, F

VI, and Ne VII, the improved calculations included mixing with the  $1s^22s^2$ ,  $1s^22s2p^1$ ,  $1s2s2p^2$ ,  $1s2s2p3s$ ,  $1s2s2p3p$ ,  $1s2s2p3d$ ,  $1s2s2p^3$ ,  $1s2p^23s$ ,  $1s2p^23p$ ,  $1s2p^33d$  and  $1s2p^34s$  mixing non-relativistic configurations. From a basis of jj-coupled states to all possible total angular momentum J from all non-relativistic configurations, the eigenvectors are regrouped in the basis of the LS terms. In the GRASP code [10], the QED effects, the self-energy and the vacuum polarization correction, are taken into account by using the effective nuclear charge  $Z_{\text{eff}}$  in the formulas of QED, which comes from an analog hydrogenic orbital with the same expectation value of r as the MCDF-orbital in question [21-25].

The transition energies and wavelengths of the  $1s2s2p^2 \ ^5P_J-1s2p^3 \ ^5S^{\circ}_2$ ,  $J=1,2,3$ , multiplets are given in Table 3.1. The non-relativistic results are from the SCHF calculation. All the calculations are compared with the experimental data available [33-36]. Data points for the deviations of transition energies and wavelengths from the experiments are evaluated and plotted in Fig. 3.1. Here, the theoretical transition energy is the center of gravity of the  $1s2s2p^2 \ ^5P_J-1s2p^3 \ ^5S^{\circ}_2$ ,  $J=1,2,3$ , transition energies computed from the fine structure transitions with the results of theoretical analysis, while the experimental transition energy is the center of gravity of the  $1s2s2p^2 \ ^5P_J-1s2p^3 \ ^5S^{\circ}_2$ ,  $J=1,2,3$ , transition energies computed from the observed transitions with the results of theoretical analysis. For the calculations the error bars are smaller than the symbols. The MCHF-plot of Fig. 3.1 is demonstrated to be linear for many transitions of nuclear charge  $Z>5$ , whereas SCHF- and MCDF-plots show that the chosen configuration basis set makes the deviation to a constant as required by theory. The values from the MCHF calculations are very close to the experiments. For C III, N IV and O V

the energy deviations are just several  $\text{cm}^{-1}$ . For F VI and Ne VII the energy deviations are less than  $200 \text{ cm}^{-1}$ . The non-relativistic results are from relativistic SCHF calculations. However, the non-relativistic transition energies are much closer to the experiments than the SCHF results. For the heavy atoms  $Z > 9$ , the non-relativistic results are good approximations. To begin with, these linear deviations can be used to predict easily and with high accuracy transitions for higher  $Z$ , in particular for Na, Mg, Al and Si although relativistic effects will become important for these elements.

The lifetimes of the upper multiplets  $1s2p^3 \ ^5S^o_2$ ,  $J=1,2,3$ , are given in Table 3.2. All the calculations are compared with the experimental data available. Data points for the deviations of lifetimes from the experiments are evaluated in Table 3.2 and plotted in Fig. 3.2. We can see the accuracy for the lifetime calculations is about 15-20 %, about the same as that of experiments.

TABLE 3.1. The energies  $E$  (in  $\text{cm}^{-1}$ ) and wavelengths  $\lambda$  (in  $\text{\AA}$ ) for the  $1s2s2p^2\ ^5P_J-1s2p^3\ ^5S^o_2$  transitions in C III, N IV, O V, F VI, and Ne VII by this work. We also list the deviations between the theoretical and experimental transition energies for the  $1s2s2p^2\ ^5P_J-1s2p^3\ ^5S^o_2$  transitions.

Ions	$\lambda$ mchf	Emchf	dEcal	$\lambda$ schf	E schf	dEcal	$\lambda$ mcdf	Emcdf	dEcal	$\lambda$ exp	Eexp	d $\lambda$ exp	dEexp
J-J'	$\pm 197$			$\pm 2796$			$\pm 264$						
C III										a	a	a	a
3-2	1016.12	98414	19	989.20	101092	2697	1015.85	98440	45	1016.31	98395	0.05	5
2-2	1015.86	98439	23	988.99	101113	2697	1015.57	98467	51	1016.09	98416	0.05	5
1-2	1015.27	98496	16	988.44	101170	2690	1015.00	98522	42	1015.43	98480	0.05	5
AVwei	1015.86	98439	20	988.98	101114	2695	1015.59	98465	46	1016.06	98419	0.05	5
AVunw	1015.75	98450	19	988.88	101125	2695	1015.47	98476	46	1015.95	98430	0.05	5
nonrel				991.24	100884	2465							
N IV										a	a	a	a
3-2	825.89	121082	18	807.50	123839	2775	824.66	121263	199	826.01	121064	0.05	7
2-2	825.36	121159	15	807.02	123913	2769	824.11	121343	199	825.46	121144	0.05	7
1-2	824.50	121285	14	806.21	124037	2766	823.28	121465	194	824.60	121271	0.05	7
AVwei	825.43	121148	16	807.08	123903	2771	824.20	121330	198	825.55	121132	0.05	7
AVunw	825.25	121175	16	806.91	123930	2770	824.02	121357	197	825.36	121160	0.05	7
nonrel				810.08	123445	2381							
O V										a	a	a	a
3-2	695.42	143798	12	682.42	146537	2751	694.70	143947	161	695.48	143786	0.10	20
2-2	694.54	143980	6	681.60	146714	2740	693.67	144161	187	694.57	143974	0.05	10
1-2	693.37	144224	-2	680.49	146953	2727	692.44	144417	191	693.36	144226	0.05	10
AVwei	694.72	143944	7	681.76	146679	2742	693.90	144112	176	694.75	143937	0.05	10
AVunw	694.44	144001	5	681.50	146734	2739	693.60	144175	180	694.47	143995	0.05	10
nonrel				685.60	145858	1922							
F VI										b	b	b	b
3-2	600.46	166539	75	590.80	169262	2798	599.78	166727	263	600.73	166464	0.08	22
2-2	599.17	166897	36	589.56	169618	2757	598.55	167069	208	599.30	166861	0.10	28
1-2	597.65	167322	42	588.10	170039	2759	597.11	167473	193	597.80	167280	0.08	23
AVwei	599.47	166815	55	589.85	169536	2776	598.84	166990	230	599.67	166758	0.10	28
AVunw	599.09	166919	51	589.49	169639	2771	598.48	167089	221	599.27	166869	0.10	28
nonrel				594.62	168175	1416							

TABLE 3.1. Continued.

Ions	$\lambda$ mchf	Emchf	dEcal	$\lambda$ schf	E schf	dEcal	$\lambda$ mcdmf	Emcdf	dEcal	$\lambda$ exp	Eexp	d $\lambda$ exp	dEexp
J-J'		$\pm 197$			$\pm 2796$			$\pm 264$					
Ne VII										c	c	c	c
3-2	528.50	189216	-160	520.64	192071	2695	527.67	189513	137	528.05	189376	0.10	36
2-2	526.71	189859	-197	518.92	192706	2650	525.71	190221	164	526.16	190056	0.10	36
1-2	524.79	190554	-176	517.08	193394	2664	523.69	190954	224	524.30	190730	0.20	73
AVwei	527.15	189698	-176	519.35	192547	2674	526.22	190035	162	526.67	189874	0.10	36
AVunw	526.66	189876	-178	518.88	192724	2669	525.69	190227	173	526.17	190054	0.10	36
nonrel				525.14	190425	546							

a Berry [33]

b Martinson [34]

c Hardis [35]

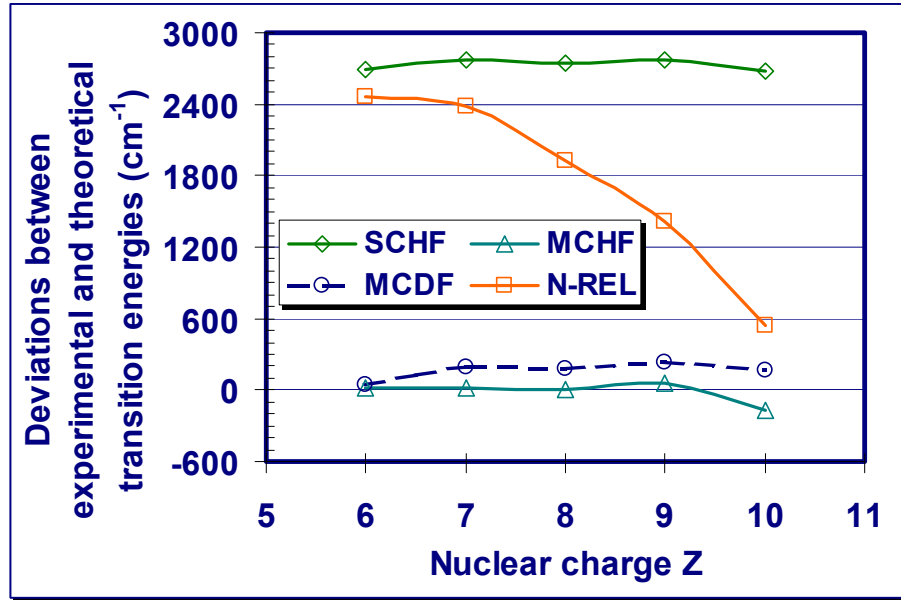


FIG. 3.1. The deviations between the theoretical and experimental transition energies for the  $1s2s2p^2 \ ^5P_J-1s2p^3 \ ^5S^o_2$  transitions. Here the theoretical transition energy is the center of gravity of the  $1s2s2p^2 \ ^5P_J-1s2p^3 \ ^5S^o_2$ ,  $J=1,2,3$ , transition energies (computed from the fine structure lines by this work) with the results of theoretical analysis, and the experimental transition energy is the center of gravity of the  $1s2s2p^2 \ ^5P_J-1s2p^3 \ ^5S^o_2$ ,  $J=1,2,3$ , transition energies (computed from the observed lines [33-35]) with the results of theoretical analysis.

TABLE 3.2. Lifetimes (in ns) of the  $1s2p^3\ ^5S_2$  states in O V, F VI and Ne VII.

Ion	This work			Expt	Theory
	MCHF $\pm 0.09$	SCHF $\pm 0.08$	MCDF $\pm 0.10$		
C III	0.54	0.36	0.35	$0.49 \pm 0.03^a$	$0.39^a$
N IV	0.35	0.29	0.29	$0.33 \pm 0.06^a$	$0.31^a$
O V	0.29	0.24	0.24	$0.21 \pm 0.02^{ab}$	$0.26^a$
F VI	0.24	0.21	0.20	$0.18 \pm 0.02^c$	$0.22^e$
Ne VII	0.21	0.18	0.17	$0.09 \pm 0.01^d$	$0.19^e$

a Berry [33]

b Livingston [37]

c Martinson [34]

d Hardis [35]

e Cheng in [33-35]

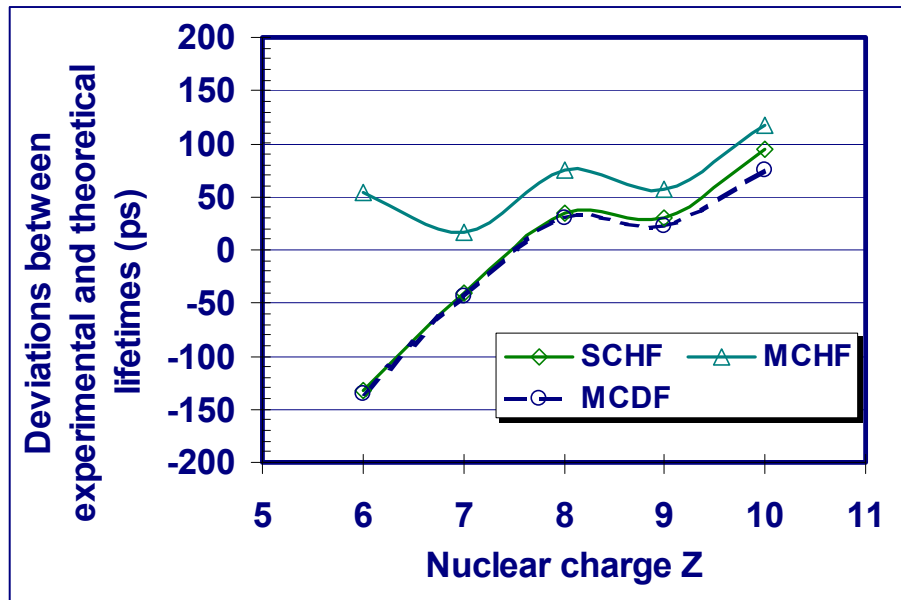


FIG. 3.2. The deviations between the theoretical (this work) and experimental [32-35,37] lifetimes for the  $1s2p^3\ ^5S_2$  state in the beryllium sequence.

Since the  $^{19}\text{F}$  nucleus has a nuclear spin  $I=1/2$ , whereas  $I=0$  for  $^{12}\text{C}$ ,  $^{14}\text{N}$ ,  $^{16}\text{O}$ ,  $^{20}\text{Ne}$ , the hyperfine structure (hfs) can be considered in a detailed analysis of the  $1s2s2p^2\ ^5\text{P}_J-1s2p^3\ ^5\text{S}^{\circ}_2$  quintet transitions. Thus, in a beam-foil study the multiplet in F V was resolved into three components due to  $F=J-1/2$  and  $F=J+1/2$  splitting of the two states. Most of the hyperfine structure is due to the Fermi contact term caused by the  $1s$  vacancy. As a starting point in the analysis, we used the theoretical values of Lunell and Beebe [38] for the three hfs parameters,  $a_c$  (contact term),  $a_1$  (orbital term) and  $a_d$  (spin-dipolar term) of the terms in F VII. In the case of F V, we can use the same values of  $a_c$  as in the F VII case because the hfs is also essentially determined by the fermi contact term of the  $1s$  electron. In the case of F VII Lunell and Beebe obtained the values (in atomic units)  $a_c=1060$  ( $^4\text{P}^{\circ}$ ),  $957.9$  ( $^4\text{P}$ ),  $a_1=21.74$ ,  $21.65$ ,  $a_d=-4.37$ ,  $-4.36$ . The contact term is clearly dominant. These theoretical values were converted into the hyperfine constant  $A_J$  (in MHz) by the equation given by Hibbert

$$A_J = G_{en} \frac{\mu_I}{I} \left( \frac{\langle \mathbf{L} \cdot \mathbf{J} \rangle}{LJ(J+1)} a_1 + \frac{3\langle \mathbf{L} \cdot \mathbf{S} \rangle \langle \mathbf{L} \cdot \mathbf{J} \rangle - L(L+1)\langle \mathbf{S} \cdot \mathbf{J} \rangle}{SL(2L-1)J(J+1)} \frac{1}{2} g_s a_d + \frac{\langle \mathbf{S} \cdot \mathbf{J} \rangle}{SJ(J+1)} \frac{1}{6} g_s a_c \right)$$

, and

$$E_{\text{hfs}} = \frac{1}{2} A_J [F(F+1) - I(I+1) - J(J+1)].$$

The numerical value of  $G_{en}$  is 95.4129 MHz. For  $^{19}\text{F}$ ,  $\mu_I=2.6287$  n.m.,  $g_s = 2 \times 1.00119652193$  and  $I=1/2$ . Because of different conventions the  $a_c$  values given by Lunell must be multiplied by 3 before they are inserted into equ. (1) [34]. Thus  $a_c=3180$  and  $2874$  should be used. No changes are needed for  $a_d$  and  $a_1$ . Furthermore, the effects of  $a_d$  and  $a_1$  are negligible in the present study. With

the above considerations we have computed the hyperfine shifts of the fine structure levels and results are shown in Fig. 3.3. The fine structures are from the MCHF calculation of this work and are shown on the left side. The right side shows the calculated hyperfine splitting, on a much-expanded scale, by this work. For the  $\Delta J=1$  transitions of F V, there are three hfs components. The  $\Delta F=0$  transition has very low intensity, which is forbidden by the selection rules for electric-dipole transitions. The energy difference between the two  $\Delta F=1$  components for  $J=3-J'=2$  transition is within about  $1 \text{ cm}^{-1}$  from the unshifted line position. The energy difference between the two  $\Delta F=-1$  components for  $J=1-J'=2$  transition is within about  $1 \text{ cm}^{-1}$  from the unshifted line position. Thus, the weighted hfs of the  $\Delta J=1$  fine structures for the transition are not observed with the experimental resolution in the Martinson's experiment [34]. However, for the  $J=2-J'=2$  transition there are four hfs components, and symmetrically placed within  $0.01 \text{ \AA}$  and  $0.1-0.3 \text{ \AA}$  around the unshifted position by the calculation of the work. In order to test this consideration for fluorine experimentally, we reviewed old spectra for the  $1s2s2p^2 \ ^5P-1s2p^3 \ ^5S$  transitions in F VI, which was at that time measured as  $599.67 \pm 0.10 \text{ \AA}$  [34] ( $597.80 \pm 0.10 \text{ \AA}$  for  $^5P_1 - ^5S_2$ ,  $599.30 \pm 0.08 \text{ \AA}$  for  $^5P_2 - ^5S_2$ , and  $600.73 \pm 0.08 \text{ \AA}$  for  $^5P_3 - ^5S_2$ ). No hyperfine structure could be observed in the experiments. The spectral width was a few times that of the calculated hyperfine structure. The nuclear spins  $I$  are zero in  $^{16}\text{O}$ ,  $^{20}\text{Ne}$  and other ions with observations considered in the thesis.

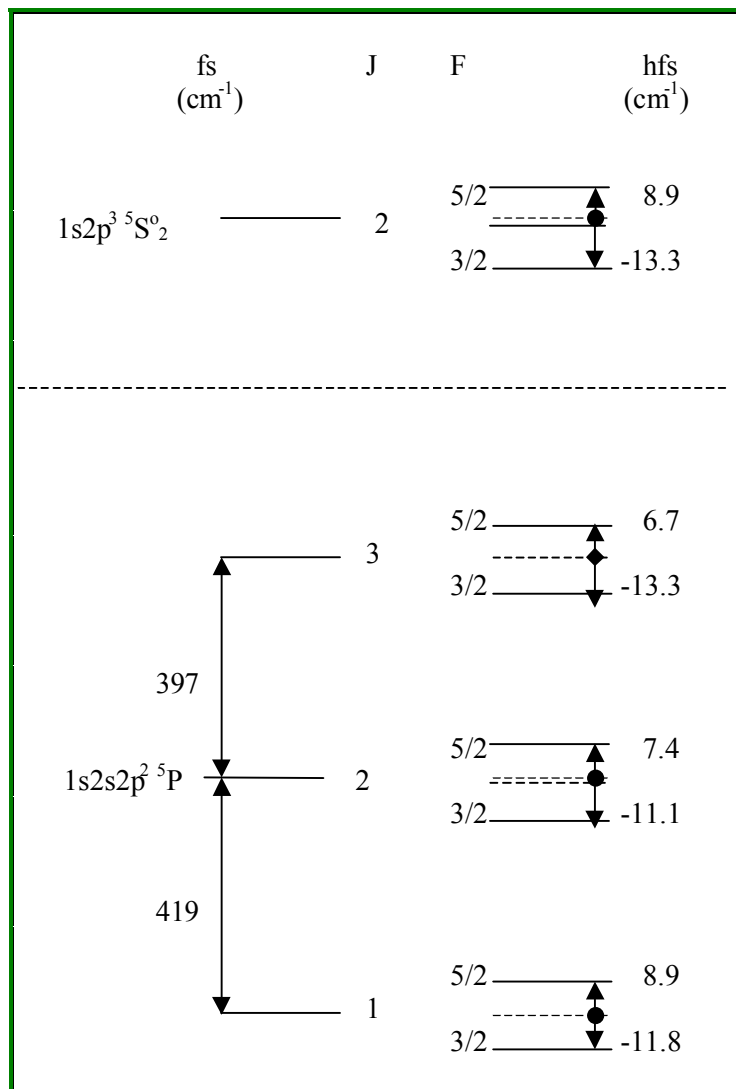


FIG. 3.3. Theoretical fine and hyperfine structure of the  $1s2s2p^2\ ^5P_{J=1,2,3}$  and  $1s2p^3\ ^5S^{\circ}_2$  states in F VI by this work.

### 3.4 The Multi-Configuration Hartree-Fock (MCHF) Calculations for Sextet States in Boron-like O IV, FV and Ne VI

#### 3.4.1 MCHF calculations for the sextet states $1s2s2p^3\ ^6S^o$ , $1s2s2p^23s\ ^6P$ and $1s2p^33s\ ^6S^o$ of boron-like O IV, F V and Ne VI

The energies, lifetimes and the relevant E1 transitions of the three doubly-excited sextet states  $1s2s2p^3\ ^6S^o$ ,  $1s2s2p^23s\ ^6P$  and  $1s2p^33s\ ^6S^o$  of boron-like O IV, F V and Ne VI were calculated with the single-Configuration Hartree-Fock (SCHF) method, and the Multi-Configuration Hartree-Fock (MCHF) (with the hydrogen-like QED and higher-order corrections) method. In the SCHF calculations only the configurations corresponding to the desired levels were considered. In the MCHF calculations four methods were explored to study the electron correlation effects. Firstly the configurations belonging to the same complex (defined with the same  $n=(n_1, n_2, n_3, n_4, n_5)$  and parity  $\pi$ ) were included (MCHF<sub>c</sub>). To study more configuration interactions for the  $1s2s2p^3\ ^6S^o$ ,  $1s2s2p^23s\ ^6P$  and  $1s2p^33s\ ^6S^o$  states we included all the configurations  $1s2l2p^2nl''$ ,  $l=s$  or  $p$ ,  $n=2,3,4$ ,  $l'=s, p, d$  or  $f$  (MCHF<sub>4</sub>), and the quasi-degenerate configurations  $1s2l2p3l'3l''$ ,  $l=s$  or  $p$ ,  $l'$  and  $l''=s, p$  or  $d$  (MCHF<sub>3</sub>). The numbers of the configurations for the ground states  $1s2s2p^3\ ^6S^o$ ,  $1s2s2p^23s\ ^6P$  and  $1s2p^33s\ ^6S^o$  of boron-like ions with MCHF<sub>c</sub> method were 1, 3 and 2, respectively. Those for MCHF<sub>4</sub> were 5, 7 and 5. Those for MCHF<sub>3</sub> were 9, 13 and 9. After updating the MCHF codes we performed the relativistic calculations with an initial expansion of up to 2000 CSFs and the full Hamilton matrix  $H$ . For a five-electron system the CI expansion generated by an active set leads to a set of large expansions. In order to reduce the number of configurations, we chose

those with the 1s electron singly occupied, i.e.  $1s n_1 l_1 n_2 l_2 n_3 l_3 n_4 l_4$ , where  $n_i=2, 3, 4$  and 5,  $l_i=0, \dots, \min(f, n_i)$ . We also included 6s and 6p electrons. We did not include the g electrons of the n=5 shell. For the calculations of the ground state  $1s2s2p^3 \ ^6S^o$  with the MCHF method we chose the 1s, 2s, 2p, 3s, 3p, 3d, 4s, 4p, 4d, 4f, 5s, 5p, 5d, 5f and 6s electrons to compose the configurations. For the  $1s2s2p^2 3s \ ^6P$  state in O IV we chose the 1s through to 5d electrons. For the  $1s2s2p^2 3s \ ^6P$  state in F V and Ne VI we chose the 1s through to 5f electrons. For the  $1s2p^3 3s \ ^6S^o$  state in O IV we chose the 1s through to 6s electrons. For the  $1s2p^3 3s \ ^6S^o$  state in F V and Ne VI we chose 1s through to 5d, 5f and 6p electrons. With these limitations we was able to obtain convergence and good results within a reasonable amount of computing time. After updating the MCHF codes we performed the relativistic calculations with the initial expansion of up to 4000 CSFs and the full Hamilton matrix H. After determining the radial wavefunctions we included the relativistic shift operators of the mass correction, the one- and two-body Darwin terms and the spin-spin contact term. The J-dependent fine structure operators were not included as suggested by Miecznik *et al.* [16]. The fine structure splittings were measured quite accurately in the experiments and identifications were determined and consistent with the SCHF and MCHF methods. The accuracy of the fine structures calculated with the SCHF method is about  $400 \text{ cm}^{-1}$ , much larger than the uncertainty of the observed transition energies and wavelengths.

TABLE 3.3. A short wavefunction expansion CI for the  $1s2s2p^3\ ^6S^o$ ,  $1s2s2p^23s\ ^6P$ ,  $1s2p^33s\ ^6S^o$ ,  $1s2s2p^23p\ ^6D^o$ ,  $1s2p^33p\ ^6P^o$ ,  $1s2s2p^23d\ ^6F$ ,  $1s2p^33d\ ^6D^o$ ,  $1s2s2p^24f\ ^6G^o$  and  $1s2p^34f\ ^6F$  states of boron-like O IV and F V.  $\sum_{i=1}^4 c_i^2$  is the

total contributions of the CSFs listed the above.

CSF	This work			Others [G. Miecjanik] [16]	
	O IV	F V	Ne VI	O IV	F V
$1s2s2p^3\ ^6S^o$					
	O IV	F V	Ne VI	O IV	F V
$1s2s2p^3$	0.99816	0.99858	0.99890		
$1s2s2p^23p$	0.00516	0.00269	-0.00133		
$1s2p3p^2$	0.00178	0.00088	-0.00081		
$1s2s2p^24p$	0.00326	0.00401	0.00510		
$\sum_{i=1}^4 c_i^2$	0.99636	0.99719	0.99783		
$1s2s2p^23s\ ^6P$					
	O IV	F V	Ne VI	O IV	F V
$1s2s2p^23s$	0.99370	0.99395	0.94589	0.99365	0.99379
$1s2s2p^23d$	-0.05209	-0.05749	-0.06024	-0.04601	-0.05773
$1s2p^33p$	0.06070	0.06424	0.03553	0.06484	0.06509
$1s2s2p^24s$	-0.00024	-0.00016	-0.17845	0.00129	-0.00083
$\sum_{i=1}^4 c_i^2$	0.99384	0.99537	0.93144	0.99366	0.99519
$1s2p^33s\ ^6S^o$					
	O IV	F V	Ne VI	O IV	F V
$1s2p^33s$	0.99178	0.96642	0.91137		
$1s2p^34s$	0.09806	-0.17303	-0.02600		
$1s2s2p^3$	0.02167	-0.01728	-0.30513		
$1s2s2p^24p$	0.00012	-0.00351	-0.15373		
$\sum_{i=1}^4 c_i^2$	0.99371	0.96422	0.94801		

The short wavefunction expansion CIs of the sextet states for O IV, F V and Ne VI are listed in Table 3.3. Here we give the reference states and the main perturbers. For the ground sextet states, the  $1s2s2p^3\ ^6S^o$  and the  $1s2s2p^23s\ ^6P$  states, the CIs belonging to the common complex increase with increasing  $Z$ , excluding Ne VI, where  $Z=10$ . For the  $1s2p^33s\ ^6S^o$  states the CIs go down with increasing  $Z$  due to the strong interactions between the  $1s2p^33l\ ^6S^o$  states. The configuration interaction increases with increasing  $Z$ . The energy calculations of the ground sextet states  $1s2s2p^3\ ^6S^o$  for the three elements O IV, F V and Ne VI are given in Table 3.4. For O IV we calculated the total energy of the ground sextet states with six different methods. For F V and Ne VI we did not obtain the  $MCHF_c$ ,  $MCHF_4$  and  $MCHF_3$  energies. Evidence indicates that the energies of the configurations in the  $MCHF_c$ ,  $MCHF_4$  and  $MCHF_3$  calculations are very close and cause the poor convergence. In a number of cases we need high energy (or frequency) components to obtain accurate wavefunctions and eigenenergies of the Breit-Pauli hamiltonian.

*TABLE 3.4. Energies (in  $cm^{-1}$ ) as well as the QED effects and higher order corrections of the  $1s2s2p3\ ^6S^o_{5/2}$  states in boron-like O IV, F V and Ne VI.*

$Z$	$E_{SCHF}$	$E^T_{SCHF}$	$E_c$	$E_3$	$E_4$	$E_{MCHF}$	$E^T_{MCHF}$
8	-11277257.8	-11276779.0	-11277257.8	-11284338.6	-11280193.7	-11285837.3	-11285376.4
	$E_{QED}$	576.7				576.9	
	$E_{HO}$	-98.0				-116.1	
9	-14626971.6	-14626257.6				-14636003.7	-14635021.2
	$E_{QED}$	881.0				881.2	
	$E_{HO}$	-167.0				101.3	
10	-18418039.2	-18416295.3				-18426807.1	-18425137.4
	$E_{QED}$	1284.7				1285.1	
	$E_{HO}$	459.2				384.6	

In chapter 5.1 we will show the detailed results and comparisons of the energies, lifetimes and the relevant E1 transitions of the doubly excited sextet states  $1s2s2p^23s\ ^6P$  and  $1s2p^33s\ ^6S^o$  of boron-like O IV, F V and Ne VI.

### *3.4.2 MCHF calculations for the $1s2s2p^23l\ ^6L-1s2p^33l\ ^6L'$ , $l=p, d$ , electric-dipole transitions of boron-like O IV, F V and Ne VI*

We next consider several  $n=3$  to  $n'=3$  transitions. The main goal of this work was to find the  $1s2s2p^23l\ ^6L-1s2p^33l\ ^6L'$ ,  $l=p, d$ , electric-dipole transitions between sextet states in O IV, FV and Ne VI. We utilized two different approaches.

In the first approach we performed the SCHF calculations. In the SCHF calculations only the configurations corresponding to the levels of the desired were considered. After updating the MCHF codes we performed the relativistic calculations with an initial expansion of up to 4000 CSFs and a full Pauli-Breit Hamiltonian matrix  $H$ . For a five-electron system the CI expansion generated by the active set leads to a large number of expansions. In order to reduce the number of the configurations, we chose the  $n_1l_1n_2l_2n_3l_3n_4l_4n_5l_5$  configurations, where  $n_i=1, 2, 3, 4$  and  $5$ ,  $l_i=0, \dots, \min(4, n_i-1)$ . We also included the  $6s$  and  $6p$  electrons. We did not include the  $g$  electrons for the  $n=5$  shell. For the  $1s2s2p^23l\ ^6L$ ,  $L=S, P, D$  for  $l=p$ , and  $L=P, D, F$  for  $l=d$  states we chose the  $1s$  through  $5s$  electrons. For the  $1s2p^33l\ ^6L$ ,  $L=P$  for  $l=p$ , and  $L=D$  for  $l=d$  we chose the  $1s$  through  $4d$  electrons. After determining the radial wavefunctions we included the relativistic operators of mass correction, one- and two-body Darwin terms and the spin-spin contact term. The fine structure splitting is strongly involved in the experiments and identifications. Hence, we included the  $J$ -dependent fine

structure operators, orbit-orbit term, spin-orbit term and spin-other-orbit term in the SCHF, SCHFT, MCHF and MCHFT calculations, which were not included earlier by Miecznik *et al.* [16].

In addition, we used the screened hydrogenic formula (3.1.25)-(3.1.30) from [25-27] to estimate the quantum electrodynamics effects (QED) and also higher-order relativistic contributions for the sextet states in five-electron oxygen, fluorine and neon.

### 3.5 The Multi-Configuration Dirac-Fock (MCDF) Calculations for Sextet States in Boron-like O IV, FV and Ne VI.

The main goal of this work was to find the  $1s2s2p^23l\ ^6L-1s2p^33l\ ^6L'$ ,  $l=s, p, d$ , electric-dipole transitions between sextet states in O IV, FV and Ne VI. We used the MCDF [21-24] program to calculate the energies, lifetimes and relevant E1 transitions of the  $1s2s2p^23l\ ^6L-1s2p^33l\ ^6L'$ ,  $l=s, p, d$ , electric-dipole transitions of boron-like O IV, F V and Ne VI. First we used the single-configuration Dirac-Fock approach (SCDF). A basis of *jj*-coupled states to all possible total angular momentum *J* from two non-relativistic configurations, like  $1s2s2p^3$  and  $1s2s2p^23s$  or  $1s2s2p^23s$  and  $1s2p^33s$ , was considered. After calculating all possible levels for all *J*, the eigenvectors were regrouped in the basis of the LS terms. To obtain better evaluations of the correlation energies of the three doubly-excited sextet states  $1s2s2p^3\ ^6S^o$ ,  $1s2s2p^23s\ ^6P$  and  $1s2p^33s\ ^6S^o$  in O IV, F V and Ne VI, the improved calculations included  $1s^22s^22p$ ,  $1s^22s2p^2$ ,  $1s2s2p^3$ ,  $1s2s2p^23s$ ,  $1s2s2p^23p$ ,  $1s2s2p^23d$ ,  $1s2p^33s$ ,  $1s2p^33p$ ,  $1s2p^33d$  and  $1s2p^34s$  mixing non-relativistic configurations.

In the GRASP code [21-24] the QED effects, the self-energy and the vacuum polarization correction, are taken into account by using the effective nuclear charge  $Z_{\text{eff}}$  in the formulas of QED, which comes from an analog hydrogenic orbital with the same expectation value of  $r$  as the MCDF-orbital in question [21-24].